Jornal of Thermal Analysis, Vol. 49 (1997) 553-565

ADSORPTION OF WATER ON ZEOLITES OF DIFFERENT TYPES

B. Hunger[1], S. Matysik[1], M. Heuchel[1], E. Geidel[2] and H. Toufar[3]

[1]Institute of Physical and Theoretical Chemistry, University of Leipzig, D-04103 Leipzig, Germany
[2]Institute of Physical Chemistry, University of Hamburg, D-20146 Hamburg, Germany
[3]Centrum voor Oppervlaktechemie en Katalyse, Katholieke Universiteit Leuven B-3001 Leuven (Heverlee), Belgium

Abstract

We have investigated the interaction of water with Na^+-ion exchanged zeolites of different structures (LTA, FAU, ERI, MOR and MFI) by means of temperature-programmed desorption (TPD). The non-isothermal desorption of water shows, depending on the zeolite type, differently structured desorption profiles. In every case the profiles have, however, two main ranges. Using a regularization method, desorption energy distribution functions have been calculated. The desorption energy distributions between 42–60 kJ mol^{-1}, which can be attributed to a non-specific interaction of water, show two clearly distinguished energy ranges. The water desorption behaviour of this range correlates with the electronegativity of the zeolites and the average charge of the lattice oxygen atoms calculated by means of the electronegativity equalization method (EEM). The part of the desorption energy distributions in the range of 60–90 kJ mol^{-1}, reflecting interactions of water with Na^+ cations, shows two more or less pronounced maxima. In agreement with vibrational spectroscopic studies in the far infrared region, it may be concluded that all samples under study possess at least two different cation sites.

Keywords: desorption energy distributions, EEM calculations, far-infrared spectroscopy, Na^+-ion exchanged zeolites of different types, temperature-programmed desorption (TPD), water adsorption

Introduction

Knowledge of interactions of water with zeolites is of great interest for their application as catalysts and adsorbents. For that thermoanalytical methods are frequently used to characterize their hydrophobic properties (e.g., [1–3]). However, non-isothermal investigations allow detailed information with respect to the strength of interaction of molecules with different adsorption sites, as it was shown for other systems (e.g., [4–6]). Therefore, we have performed temperature-programmed desorption (TPD) of water on Na^+-ion exchanged zeolites of different types in order to characterize their adsorption properties with respect to water as probe molecule in more details. Electronegativities and partial charges of the lattice oxygen atoms have been calculated with the electronegativity equalization method

0368–4466/97/ $ 5.00

John Wiley & Sons Limited
Chichester

(EEM) in order to correlate the TPD results with chemical and structural properties of the zeolites. The results for the interaction of water with the Na^+-cations will be discussed together with far infrared spectroscopic observations.

Experimental

Zeolites

The zeolites were commercially available materials supplied by the Bitterfeld AG (Germany). The characteristics are summarized in Table 1, whereby the zeolites are arranged with decreasing aluminium content. The pore volumes were determined by the gravimetric uptake of *n*-hexane at 298 K.

Temperature-programmed desorption (TPD)

The temperature-programmed desorption (TPD) was carried out in a conventional flow device with helium as carrier gas (3 l h^{-1}). For evolved gas detection both a thermal conductivity detector (TCD) and a quadrupole mass spectrometer (Leybold, Transpector CIS System) with a capillar-coupling system were used. The zeolites were equilibrated with water vapour over a saturated $Ca(NO_3)_2$ - solution in a desiccator. For each experiment 20–100 mg of the water loaded zeolite were used in a mixture with 1 g quartz of the same grain size (0.2 ... 0.4 mm). At first all samples were flushed with helium at room temperature for a period of 40 min. Afterwards the linear temperature program (10 K min^{-1}) was started. For a kinetic evaluation experiments were carried out using different heating rates (2 ... 20 K min^{-1}). In some investigations the adsorption was performed by means of a water vapour pulse and an isothermal desorption of the water surplus.

The adsorbed water amounts (Table 1) were determined additionally by a simultaneous thermal analysis apparatus (TG-DTA-QMS, NETZSCH, System STA-QMS 409/403). For all of these experiments the sample weight was about 40 mg. A heating rate of 10 K min^{-1} and a helium flow of 4.5 1 h^{-1} were used.

Far-infrared spectroscopic investigations

Samples were pressed to form self-supporting wafers and dehydrated in a far-IR cell with polyethylene windows in a stream of dry nitrogen at 623 K. After cooling measurements of the far infrared spectra were carried out in a nitrogen atmosphere as well for suppression of rotational lines of water vapour. Absorption spectra at room temperature were recorded using a Digilab FTS 15E spectrometer, equipped with a mercury vapour source, a 6.25 μm mylar beamsplitter and a liquid-helium-cooled silicon bolometer (Infrared Laboratories) as high sensitive detector. Spectra were taken in the range 400–20 cm^{-1} with a resolution of 4 cm^{-1} coadding 256 scans to obtain an acceptable signal-to-noise ratio. A triangle apodization function was applied for the Fourier transformation.

Table 1 Characteristics of zeolites

Zeolite	Structure type code	Chemical composition	Si/Al-ratio	Pore volume/ $cm^3\ g^{-1}$	Water adsorption capacity at 298 K/ $mmol\ g^{-1}$
NaA	LTA	$Na_{12}[Al_{12}Si_{12}O_{48}]$	1	0.287	14.43
NaX	FAU	$Na_{88.1}[Al_{88.1}Si_{103.9}O_{384}]$	1.18	0.311	16.55
NaY	FAU	$Na_{53.3}[Al_{53.3}Si_{138.7}O_{384}]$	2.6	0.310	16.25
Na, K-erionite	ERI	$Na_{4.89}K_{4.11}[Al_9Si_{27}O_{72}]$	3	0.190	8.83
Na-mordenite	MOR	$Na_8[Al_8Si_{40}O_{96}]$	5	0.169	7.01
NaZSM-5	MFI	$Na_6[Al_6Si_{90}O_{192}]$	15	0.102	4.25

Calculations

Crystal structures

Crystal structure calculations were carried out on zeolite NaA (Si/Al=1), NaX (Si/Al=1), NaY (Si/Al=3) and Na-mordenite (Si/Al=5). The spacegroups of the structures were reduced to F43c for LTA, F23 for FAU and $P2_1/m$ for MOR in order to allow the insertion of aluminum atoms obeying Löwensteins rule. The resulting structures were optimized using the DLS package [7] with the following parameters: Si–O distance =0.161 nm, Al–O distance =0.174 nm, O–T–O angle = 109.5°, T–O–T angle =145°. The cations were placed into the unit cells using literature data [8] in order to (i) maximize the inter-cationic distance and to (ii) maximize the coordination by lattice oxygens. The local position of the cations were adjusted during the EEM calculations at the minimum of the electrostatic energy.

EEM calculations

The electronegativity equalization method (EEM) allows the calculation of electronegativities and atomic charges in molecules as well as in large clusters and infinite crystal structures, when the structure and chemical composition are known. For a detailed description of the EEM and its applications [9–11], its predecessors [12] and its rigorous derivation in the density functional theory [13], we refer to the original literature. For the present calculations a combined Monte Carlo/EEM procedure [14] was applied. This program allows to optimize the cation positions within the crystal structure on the base of the total electronic energy of the system, i.e., including the electrostatic interactions as well as the charge dependent self-energy of the atoms. Long range effects were taken into account by a Taper type summation during the optimization. After the energy of the system had reached a minimum, the calculation of the relevant parameters was redone applying a more accurate Bertaut type summation. The results were, however, identical within the margins of the numerical error of the program. The zeolite lattice was assumed to be rigid during all computations. Three different scenarios were applied for the charge transfer between lattice and cations: (i) cations were not included into the EEM calculations, the total charge of the lattice was set zero arbitrarily; (ii) free charge transfer was allowed between zeolite lattice and cations; (iii) the charge of the cations was fixed to +1 and the total charge of the lattice was fixed to the corresponding negative value ($q_{\text{lattice}} = -\Sigma q_{\text{cation}}$). Scenario (i) allows to separate the influence of the zeolite structure partially from the effect of the chemical composition. However, since in practice the effect of the composition will always be dominating, these results cannot be correlated directly to experimental results. The scenario (ii) is the physically most realistic one. Unfortunately, the determination of accurate EEM parameter for alkali-metals is still an unsolved problem, mostly due to the discontinuity of these parameters at a charge of +1 [15]. Therefore, it is more suitable in most cases to apply scenario (iii) as a fairly good approximation of the reality. In this case, EEM parameters for the cations are not required. Only the electrostatic polarization of the lattice by the cations is taken into account in this way, while the

Table 2 Desorbed water amounts in different temperature ranges and results of EEM calculations

Zeolite	300–700 K/ mmol g^{-1}	450/500–700 K/ mmol g^{-1}	Electronegativity	Average charge of lattice oxygen atoms
NaA	10.2	2.1	–3.79	–0.89
NaX	10.3	2.5	–1.87	–0.88
NaY	9.9	1.7	2.4	–0.84
Na, K-erionite	6.8	1.4	n.c. [1]	n. c.
Na-mordenite	6.5	2.0	1.74	–0.85
NaZSM-5	2.8	1.2	n.c.	n. c.

[1] n.c.: not calculated

charge transfer part is ignored. Ab initio calculations on alkali cation – water systems indicate, however, that the charge transfer between the cations and coordinating oxygen atoms is rather small [16]. The electronegativities calculated by means of scenario (iii) and the predicted average charge of the lattice oxygen atoms are summarized in Table 2.

Results and discussion

For all zeolites the desorption curves of water are shown in Fig. 1. In each case, reversibility could be proofed by performing repeated adsorption/desorption cycles. The mass-spectroscopic analysis (H_2O: 18 amu; CO_2: 44 amu; N_2: 28 amu; O_2: 32 amu) showed that only water was desorbed. Characteristic for all zeolites are two clearly visible ranges of desorption. The predominant amount of water desorbs up to about 400–450 K. Smaller amounts desorb between about 450–500 K and about 700 K. The amount of water desorbing in this temperature range was separated from desorption up to about 450 K by combination of isothermal and non-isothermal desorption. For this purpose, heating was carried out up to the first peak maximum and then the temperature program was stopped. When no further desorption was observed at this temperature, the temperature program was restarted. The obtained desorption curves are shown in Fig. 2 and the desorbed amounts are summarized in Table 2. A comparison with the adsorbed amounts determined at saturation pressure in the desiccator (Table 1) shows that during flushing with helium at room temperature already 25–40 % of water desorbs before the TPD was started. Therefore, the TPD allows information especially with respect to low initial coverage. This should be an advantage in comparison to isothermal adsorption measurements,

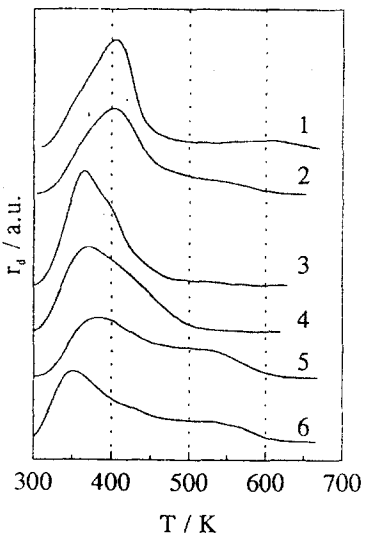

Fig. 1 Desorption curves of water: 1: NaA, 2: NaX, 3: NaY, 4: Na,K-erionite, 5: Na-mordenite, 6: NaZSM-5

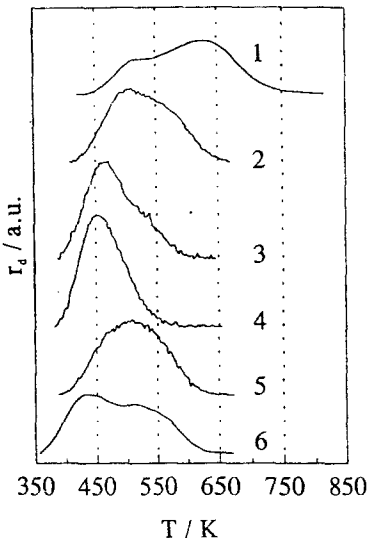

Fig. 2 Desorption curves after isothermal desorption: 1: NaA, 2: NaX, 3: NaY, 4: Na,K-erionite, 5: Na-mordenite, 6: NaZSM-5

where this range is relatively difficult to investigate, especially, because of the very small equilibrium pressures.

In order to obtain detailed information about the desorption process a further evaluation of the experimental curves was carried out. For this purpose a rate law of first order with a distribution function $f(E)$ of desorption energy E was considered [17]:

$$r_d = -\frac{d\theta}{dt} = A\int_{E_{min}}^{E_{max}} \theta_l(E,T)\, \exp(-E/RT)\, f(E)\, dE \qquad (1)$$

where r_d is the overall desorption rate, θ is the overall degree of coverage, and A the pre-exponential factor. θ_l is the local coverage of sites characterized by a desorption energy E. E_{min} and E_{max} are the limits of the range of desorption energy. The calculations were carried out by means of the program INTEG [18], which involves a regularization method for solving this integral equation.

The pre-exponential factor A required to solve Eq. (1) was estimated by using the dependence of the temperature of the peak-maximum on the heating rate [19, 20]. For NaZSM-5 the pre-exponential factor was determined to be between 2×10^6 and 1×10^7 min^{-1} [6]. The value for NaX was between 7×10^6 and 2×10^7 min^{-1}. This range nearly corresponds to the accuracy of estimation of these parameters. On the other hand the pre-exponential factor represents an effective parameter containing also contributions of the mass transport [21]. Therefore, a dependence on the sample amount can not be excluded. But, different sample amounts were necessary to

ensure, that similar amounts of water desorb, and the experimental conditions could be kept comparable. Because the shape of the desorption energy distribution is not significantly influenced by the value of the pre-exponential factor [17], a constant value of 5×10^6 min^{-1} was assumed for all zeolites. The resulting error is of the order of 7–8 % .

The numerical solution of Eq. (1) by means of the INTEG program was carried out without any assumptions or constraints about the resulting distribution func-

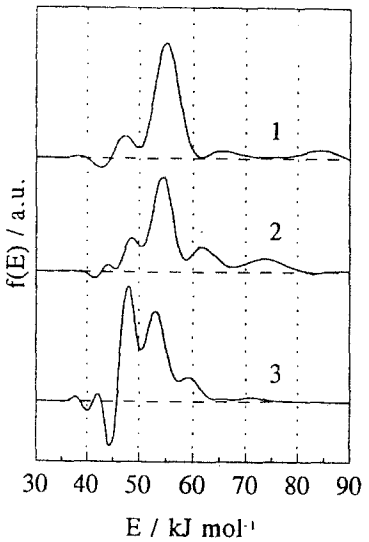

Fig. 3 Desorption energy distributions: 1: NaA, 2: NaX, 3: NaY

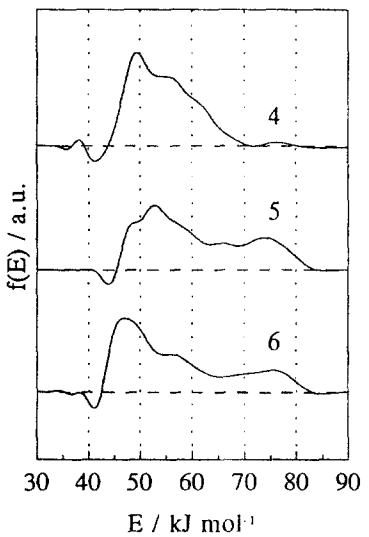

Fig. 4 Desorption energy distributions: 4: Na,K-erionite, 5: Na-mordenite, 6: NaZSM-5

tions. Thus negative parts in the distributions are possible. They fail to possess any physical meaning, but if the distribution is dominated by the negative parts, the used local model does not describe appropriately the experimental data. The negative parts are neglected in the interpretation of the distribution functions.

The calculated desorption energy distribution functions are presented in Figs 3 and 4. The energy range of about 42 to 90 kJ mol^{-1} agrees well with reported heats of adsorption on comparable zeolites for the respective coverage with water (e.g., [22–24]). Therefore, the distribution functions seem to be a useful measure to characterize the interaction strength of water very detailed. As can be seen clearly, the distribution functions are differently structured in dependence on the zeolite type. Except for NaZSM-5, all energy distributions consist of four, different superposed ranges. The two maxima at about 47–49 kJ mol^{-1} and about 52–55 kJ mol^{-1}, appearing with different frequency, correspond to water desorbing up to about 450–500 K. This water can be attributed to non-specific interactions with the zeolitic framework (lattice oxygen). Similar values for heats of adsorption have been found for water on solids with the same structure but without specific adsorption sites, e.g., cations (e.g., silicalite [25]). For Na,K-erionite, the range with the highest energy appears only as a shoulder. The lowest energy range for Na-mordenite also appears as a shoulder. In the case of NaZSM-5 this part of the distribution function is a very broad peak only. Summarized, the energy range between 42–60 kJ mol^{-1} should indicate the influence of both aluminium-content and framework structure on the strength of water interaction.

Considering the peak temperature of the desorption curve as an average measure for the strength of interaction a good linear correlation with the calculated electronegativity was found, as can be seen in Fig. 5. A similar correlation of the peak temperature was found in dependence on the mean charge of lattice oxygen atoms (Table 2), which also measures the basicity of zeolites.

However, an essential property of the desorption energy distributions in Figs 3 and 4 is the different intensity in the two energy ranges at 42–50 kJ mol^{-1} and 50–60 kJ mol^{-1}. The interpretation of the relative ratio of these intensities should give

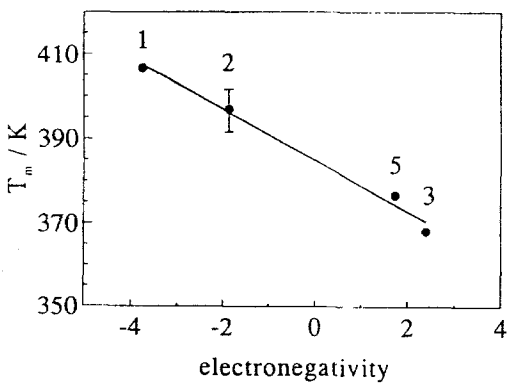

Fig. 5 Peak temperature in dependence on the electronegativity: 1: NaA, 2: NaX, 3: NaY, 5: Na-mordenite

a more comprehensive picture of the energetic heterogenity. For all zeolites distinct calculated charge values result for oxygen atoms at different crystallographic positions. For NaA and NaX, where energies in the second range of higher desorption energy appear with more intense frequency (curves 1 and 2 in Fig. 3), larger partial charges predominate. In contrast, lower partial charges are more frequent for NaY. In that case, the first range of lower desorption energies (curve 3 in Fig. 3) appears with higher intensity. For Na-mordenite the partial oxygen charges are distributed relatively uniformly. Therefore, it may be supposed that a correlation exists between the relative frequency of the two energy ranges of the desorption energy distributions and the basicity (electronegativity) of the zeolites. For that the distribution functions beween 40–60 kJ mol^{-1} were fitted by two Gaussian functions. Figure 6 shows, that with increasing electronegativity (decreasing basicity of framework) the relative frequency of the lower energy range, determined by the peak areas of the Gauss-peaks, increases.

Both correlations (Figs 5 and 6) show that Na-mordenite has a higher basicity than it would correspond to its aluminium content (see also Table 2, where the zeolites are arranged with decreasing aluminium content). The exceptional strong basicity of this zeolite type was also shown for pyrrole adsorption by means of infrared spectroscopic investigations [26].

The part of the distribution function between 60–90 kJ mol^{-1} can be assigned to interaction with Na^+-cations. Typically, the distributions show two extended energy ranges with frequencies and positions characteristic for each zeolite type. If the desorption energy distributions are calculated with the desorption curves of Fig. 2, both energy ranges become visible also for Na,K-erionite and Na-mordenite. The reason for the resulting heterogeneity seems to be the different localization of the cations.

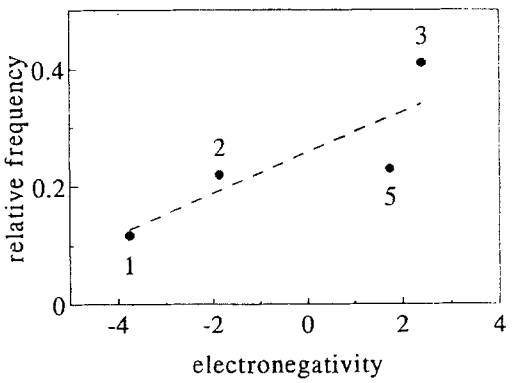

Fig. 6 Relative frequency of the low energy range (42–50 kJ mol^{-1}) in dependence on the electronegativity: 1: NaA, 2: NaX, 3: NaY, 5: Na-mordenite

Information about these extra-framework cation locations and their occupancy are usually obtained by diffraction measurements. However, for high-silica zeolites

problems arise due to the low cation concentration. So it seems appropriate to employ other methods yielding additional information on cations in zeolites such as solid-state NMR [27] or vibrational spectroscopic techniques. Vibrational spectroscopic studies in the far infrared region provide access to the normal modes of the cations with respect to the framework [28–31]. Because zeolites reveal a characteristic spectral pattern in the far infrared, several attempts have been made to relate these features with vibrational modes of cations on distinct sites [30, 32]. Although

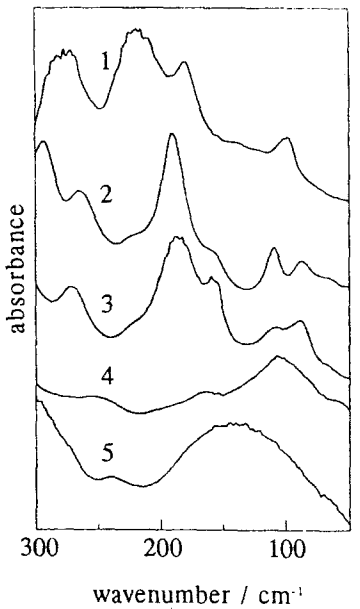

Fig. 7 Far-infrared spectra of the dehydrated zeolites: 1: NaA, 2: NaX, 3: NaY, 4: Na,K-erionite, 5: Na-mordenite

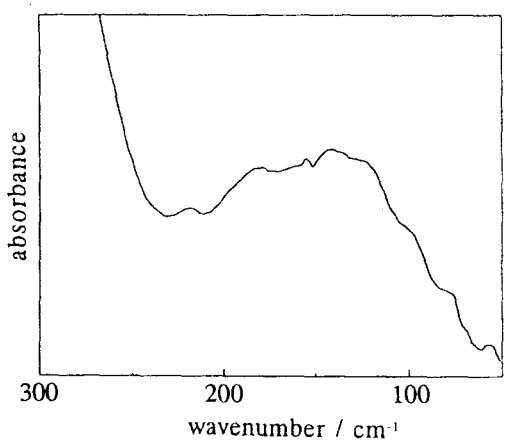

Fig. 8 Far-infrared spectrum of dehydrated NaZSM-5

recent studies have turned out the oversimplification of this model, each cation site gives a distinct spectral pattern below 250 cm^{-1} summing up to the observed far infrared spectra [33–36].

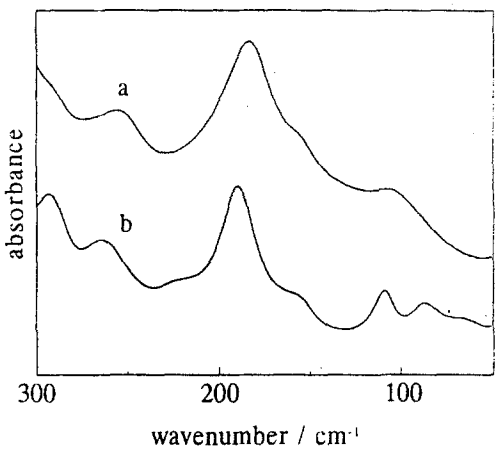

Fig. 9 Far-infrared spectra of NaX: a: hydrated sample, b: dehydrated sample

The far infrared spectra of dehydrated Na^+-ions containing zeolites with quite different lattice structures and different Si/Al-ratios are shown in Figs 7 and 8. As can be seen, with increasing cation content the number of observed bands increases in the region below 250 cm^{-1} attributable to cation vibrations. In general this can be regarded to be indicative of an increasing occupation of different cation sites with increasing heterogeneity. The observed spectrum of the zeolite NaZSM-5 exhibit two bands near 180 and 145 cm^{-1} (Fig. 8). Recently from a joined application of far infrared and X-ray absorption spectroscopy two different sites of cations were deduced for a series of MFI type zeolites [37]. Regarding this, at least two different cation sites for samples under study can be concluded on the basis of all spectra. This conclusion should be transferable to the hydrated state of sodium-containing zeolites, too, because no significant changes were obtained during water adsorption in the far infrared spectra. As can be seen in Fig. 9 for NaX, after hydration of the sample the bands become less resolved and some shifts in position occur. No new bands were, however, observed. Similar results were obtained by a FTIR study of the dehydration of Y zeolites with different monovalent cations [38]. Even if the adsorption of water may influence the cation location resulting in a redistribution, it should not provide a decrease of heterogeneity.

* * *

The authors gratefully acknowledge the partial financial support of the Fonds der Chemischen Industrie and the Deutsche Forschungsgemeinschaft, Physical Chemistry of Interfaces - Graduate College. H.T. is grateful for a Human Capital and Mobility grant of the European Commission.

References

1 M. W. Anderson and J. Klinowski, J. Chem. Soc., Faraday Trans. I, 82 (1986) 1449.
2 J. Weitkamp, P. Kleinschmit, A. Kiss and C. H. Berke, Proceedings of the 9th International Zeolite Conference, Montreal, 1992, Vol. II, (Eds: R. von Ballmoos, J. B. Higgins, M. M. J. Treacy), Butterworth-Heinemann, 1993, p. 79.
3 G. Debras, A. Gourgue, J. B. Nagy and G. De Clippeleir, Zeolites, 5 (1985) 377.
4 E. Dima and L. V. C. Rees, Zeolites, 7 (1987) 219.
5 B. Hunger, J. Hoffinann, O. Heitzsch and M. Hunger, J. Thermal Anal., 36 (1990) 1379.
6 B. Hunger, M. Heuchel, S. Matysik, K. Beck and W.-D. Einicke, Thermochim. Acta, 269/270 (1995) 599.
7 C. Baerlocher, A. Hepp and W. M. Meier, DLS-76: A Program for the Simulaton of Crystal Structures (ETH Zurich, Switzerland 1978).
8 W. J. Mortier, Compilation of Extra Framework Sites in Zeolites, Butterworth Scientific Ltd., Guildford, 1982.
9 W. J. Mortier, S. K. Ghosh and S. Shankar, J. Am. Chem. Soc., 108 (1986) 4315.
10 W. J. Mortier, Structure and Bonding, 66 (1987) 125.
11 W. J. Mortier, K. A. Van Genechten and J. Gasteiger, J. Am. Chem. Soc., 107 (1985) 829.
12 R. T. Sanderson, J. Am. Chem. Soc., 74 (1952) 272.
13 R. G. Parr, R. A. Donnelly, M. Levy and W. E. Palke, J. Chem. Phys., 68 (1978) 3801.
14 H. Toufar, B. G. Baekelandt, G. O. A. Janssens, W. J. Mortier and R. A. Schoonheydt, J. Phys. Chem., 99 (1995) 13876.
15 K. D. Sen, T. V. Gayatri and H. Toufar, J. Mol. Struc. (THEOCHEM), 361 (1996) 1.
16 H. Kistenmacher, H. Popkie and E. Clementi, J. Chem. Phys., 58 (1973) 1689.
17 B. Hunger, M. von Szombathely, J. Hoffmann and P. Brauer, J. Thermal Anal., 44 (1995) 293 .
18 M. von Szombathely, P. Bräuer and M. Jaroniec, J. Comput. Chem., 13 (1992) 17.
19 P. T. Dawson and Y. K. Peng, Surface Sci., 33 (1972) 565.
20 B. Hunger and J. Hoffmann, Thermochim. Acta, 106 (1986) 133.
21 E. Tronconi and P. Forzatti, Chem. Engng. Sci., 42 (1987) 2779.
22 M. M. Dubinin, A. A. Isirikjan, G. U. Rachmatkariev and V. V. Serpinski, Izv. Akad. Nauk SSSR, Ser. Khim., 10 (1972) 1269.
23 M. M. Dubinin, A. A. Isirikyan, G. U. Rachmatkariev and V. V. Serpinski, Izv. Akad. Nauk SSSR, Ser. Khim., 4 (1973) 934.
24 P. L. Llewellyn, N. Pellenq, Y. Grillet, F. Rouquerol and J. Rouquerol, J. Thermal Anal., 42 (1994) 855 .
25 F. Vignè-Maeder and A. Auroux, J. Phys. Chem., 94 (1990) 316.
26 B. L. Su and D. Barthomeuf, Appl. Catal., 124 (1995) 81.
27 G. Engelhardt, M. Hunger, H. Koller and J. Weitkamp, Stud. Surf. Sci. Catal., 80 (1994) 421.
28 I. A. Brodskii, S. P. Zhdanov and A. E. Stanevich, Opt. Spectrosc., 30 (1971) 58.
29 W. M. Butler, C. L. Angell, W. McAllister and W. M. Risen, J. Phys. Chem., 81 (1977) 2061.
30 M. D. Baker, G. A. Ozin and J. Godber, Catal. Rev.-Sci. Eng., 27 (1985) 591.
31 C. Brèmard and M. Le Maire, J. Phys. Chem., 97 (1993) 9695.
32 J. Godber, M. D. Baker and G. A. Ozin, J. Phys. Chem., 93 (1989) 1409.
33 K. S. Smirnov, M. Le Maire, C. Brèmard and D. Bougeard, Chem. Phys., 179 (1994) 445.
34 C. Brèmard and D. Bougeard, Adv. Mater., 7 (1995) 10.
35 K. Krause, E. Geidel, J. Kindler, H. Förster and H. Böhlig, J. Chem. Soc., Chem. Commun., (1995) 2481.
36 K. Krause, E. Geidel, J. Kindler, H. Förster and K. S. Smirnov, Vibr. Spectrosc., 12 (1996) 45.
37 H. Esemann, H. Förster, E. Geidel and K. Krause, Microporous Mater., accepted.
38 W. P. J. H. Jacobs, J. H. M. C. van Wolput and R. A. van Santen, Zeolites, 13 (1993) 170.